

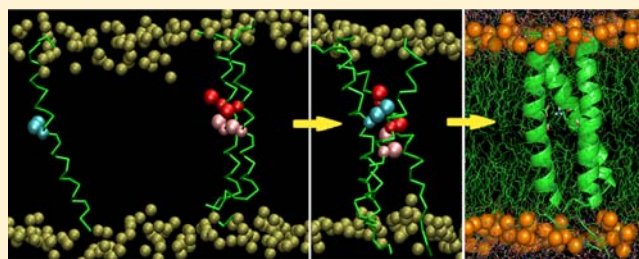
An Atomistic Model for Assembly of Transmembrane Domain of T cell Receptor Complex

Satyan Sharma and André H. Juffer*

Biocenter Oulu and Department of Biochemistry, University of Oulu, P.O. Box 3000, Oulu FI-90014, Finland

S Supporting Information

ABSTRACT: The T cell receptor (TCR) together with accessory cluster of differentiation 3 (CD3) molecules (TCR–CD3 complex) is a key component in the primary function of T cells. The nature of association of the transmembrane domains is of central importance to the assembly of the complex and is largely unknown. Using multiscale molecular modeling and simulations, we have investigated the structure and assembly of the TCR α –CD3 ϵ –CD3 δ transmembrane domains both in membrane and in micelle environments. We demonstrate that in a membrane environment the transmembrane basic residue of the TCR closely interacts with both of the transmembrane acidic residues of the CD3 dimer. In contrast, in a micelle the basic residue interacts with only one of the acidic residues. Simulations of a recent micellar nuclear magnetic resonance structure of the natural killer (NK) cell-activating NKG2C–DAP12–DAP12 trimer in a membrane further indicate that the environment significantly affects the way these trimers associate. Since the currently accepted model for transmembrane association is entirely based on a micellar structure, we propose a revised model for the association of transmembrane domains of the activating immune receptors in a membrane environment.



INTRODUCTION

One of the most important molecular driving forces for the assembly of activating immune receptors originates from the electrostatic network located in the transmembrane (TM) domains of these receptors.¹ The lack of structures of TM domains has limited our current understanding of the assembly and functioning of these domains. One of the important members of the activating immune receptors is the T cell receptor (TCR), used as a model system to understand the TM interactions in the present study.

TCR is an essential receptor for proper T cell development and functioning.² The receptor is composed of two chains, α and β , which are linked by an interchain disulfide bridge. Each chain consists of an extracellular part, a TM helical domain, and a very short intracellular region. The extracellular part contains a variable and a constant immunoglobulin (Ig)-like domain. The variable regions of both chains jointly form a ligand binding pocket.^{3,4} TCR associates noncovalently with a set of integral membrane proteins, known as the cluster of differentiation 3 (CD3) molecules. The binding of ligands (antigens) to the extracellular part of TCR triggers the signal transducing events through these CD3 molecules: CD3 $\epsilon\delta$, CD3 $\epsilon\gamma$, and CD3 $\zeta\zeta$ dimers. The CD3 proteins have an extracellular Ig-like domain (except for the CD3 $\zeta\zeta$ homodimer) and are connected to the immunoreceptor tyrosine-based activation motifs (ITAMs) bearing cytoplasmic tails via a TM region that spans the membrane once. Despite the importance of TCR and the CD3 proteins, the molecular and structural features of the association of TCR with CD3 are still not clearly understood.^{3,5}

Using *in vitro* translation followed by sequential immunoprecipitation techniques, Call et al. have characterized the TCR–CD3 assembly intermediates.⁶ Their studies demonstrated that TCR α can associate with the CD3 $\epsilon\delta$ dimer to form a stable trimer. Similarly, the TCR β has been shown to stably associate with the CD3 $\epsilon\gamma$ dimer. A charged residue present within the Asp/Glu-XX-Thr motif (XX typically are hydrophobic residues) of the TM regions of the CD3 proteins was found to be important for the assembly of trimers.^{6–8} The TCR α has two positively charged residues, an arginine (Arg13 α) and a lysine (Lys18 α) residue. The two aspartic acid residues of CD3 $\epsilon\delta$ heterodimer (referred to herein as Asp14 ϵ of CD3 ϵ chain and Asp14 δ of CD3 δ chain) are possibly involved in the interaction with the TM lysine of TCR α only, because mutation of the arginine had no effect on the extent of trimerization. Similar observations were also made for the formation of TCR β –CD3 ϵ –CD3 γ trimers, wherein a lysine on TCR β interacts with an aspartic–glutamic acid pair on the CD3 $\epsilon\gamma$ heterodimer.⁶ Further biochemical studies on other activating immunoreceptors suggest that the electrostatic interactions among the TM domains are important for their assembly.⁹

A recent NMR structure of the DNAX-activation protein 12 (DAP12) homodimer with the natural killer cell-activating receptor (NKG2C) in a micelle only partially supports the viewpoint on TM electrostatic interactions because the NMR

Received: August 24, 2012

Published: January 15, 2013

structure shows that the two TM aspartic acid residues of DAP12 dimer lie nearly opposite to each other, and only one of the acidic residues is in direct contact with the basic residue of the NKG2C.⁸ In contrast, experimental data clearly demonstrate that there is a strict requirement of a pair of acidic residues for the assembly of the trimer.^{8,9} Based on the NMR structure of the trimer, a generalized model for the assembly of immune receptors had been put forth.⁸ This model proposes that the basic residue, without any preference for either of the acidic residues, can associate with the DAP12 on either side, implying that the extracellular domains of these receptors can associate either way as well. This may contradict the notion that the specificity of interactions between residues in the TM region can explain or even direct the proper assembly of multichain membrane complexes.¹⁰ However, the aforementioned model by Call et al. only results in a 50% chance that the trimer is properly assembled, which introduces degeneracy in this particular model. This observation warrants a deeper investigation of the details of helical interactions in the membrane.

In silico modeling and simulation techniques are an important tool in gaining insight into the atomic details of the structure and functioning of macromolecules. The development of coarse-grained (CG) force fields for molecular simulation has provided the ability to attain longer time scales and to address larger systems. Among other techniques, computational methods have been successfully employed to obtain an unprecedented insight into the structure and functioning of proteins in a membrane environment.^{11–14} The present work employs these simulation techniques for studying the details of the intramembrane interactions that have been proposed to be important for the assembly of the TCR α –CD3 ϵ –CD3 δ trimer. To investigate the assembly process in a model membrane, self-assembly simulations were performed. To validate our results based on the bilayer simulations and to further improve the understanding of previous experimental observations, the TCR α –CD3 ϵ –CD3 δ trimer was also studied in a micelle environment. For comparison purposes, the assembly of NKG2C–DAP12–DAP12 trimer was studied as well. On the basis of the obtained results, we propose a revised model for the assembly of the immunoreceptor complex.

COMPUTATIONAL DETAILS

Initial Models and System Setup. The sequences used (see Figure 1) to model the TM regions of each monomer were NLNLFQNLVSMGLRILLKLVAGFNLLMTLRLWSS (TCR α), EVDLTAVAIIVDICITLGLLMVIYWSKNRK (CD3 ϵ), and ELDSGT MAGVIFIDLIATLLLALGVYCFAGHET (CD3 δ). To date, no experimental structural models are available. A helical secondary structure was assigned to residues 5–30 of TCR α , 4–27 of CD3 ϵ , and 4–27 of CD3 δ , based on various TM structure prediction programs (TMHMM2.0,¹⁵ Split4.0,¹⁶ and MINNOU¹⁷) and proposed TM regions in the literature.^{18,19} The atomistic structures of the TM domains were generated using Modeller²⁰ and subsequently energy minimized. The coordinates for the NKG2C–DAP12–DAP12 trimer were obtained from a NMR structure (deposited in the protein data bank (PDB)²¹ as entry 2L35.pdb). The obtained structures were employed in various computer simulations, listed in Table 1, the details of which are explained below. All simulations were carried out with the GROMACS MD package (version 4.0.7).²²

The CD3 ϵ –CD3 δ dimer was studied in two different bilayers, namely, in palmitoyl-oleoyl phosphatidylcholine (POPC) and dipalmitoyl phosphatidylcholine (DPPC). To assess the orientation and stability of the dimer in a bilayer, the monomeric helices were inserted parallel to each other in a pre-equilibrated bilayer, such that

NLNLFQNLVSMGLRILLKLVAGFNLLMTLRLWSS	TCR α
-----HHHHHHHHHHHHHHHHHHHHHHHHHHHH--	TMHMM
-----HHHHHHHHHHHHHHHHHHHHHHHHHHHH--	split4.0.
-----HHHHHHHHHHHHHHHHHHHHHHHHHHHH--	MINNOU
-----HHHHHHHHHHHHHHHHHHHHHHHHHHHH--	Bonifacino et. al.
CCCSHHHHHHHHHHHHHHHHHHHHHHHHHHHSSCC	This work
EVDLTAVAIIVDICITLGLLMVIYWSKNRK	CD3 ϵ
-----HHHHHHHHHHHHHHHHHHHHHHHHHHHH--	TMHMM
-----HHHHHHHHHHHHHHHHHHHHHHHHHHHH--	split4.0.
-----HHHHHHHHHHHHHHHHHHHHHHHHHHHH--	MINNOU
-----HHHHHHHHHHHHHHHHHHHHHHHHHHHH--	Chenqi et. al.
CCSHHHHHHHHHHHHHHHHHHHHHHHHHHSSCCCC	This work
ELDSGT MAGVIFIDLIATLLLALGVYCFAGHET	CD3 δ
-----HHHHHHHHHHHHHHHHHHHHHHHHHHHH--	TMHMM
-----HHHHHHHHHHHHHHHHHHHHHHHHHHHH--	split4.0.
-----HHHHHHHHHHHHHHHHHHHHHHHHHHHH--	MINNOU
-----HHHHHHHHHHHHHHHHHHHHHHHHHHHH--	Chenqi et. al.
CCSHHHHHHHHHHHHHHHHHHHHHHHHHHSSCCCC	This work

Figure 1. The TM sequences used in this study and results from various secondary structure prediction programs. The figure also shows the secondary structure assignment used for this study. Top panel, TCR α ; middle panel, CD3 ϵ ; bottom panel, CD3 δ .

the center of mass of the helices lie at a distance of 13 Å. The overlapping lipids were then removed. All manipulations were done with the VMD program.²³ After an initial 1000 steps of steepest descent energy minimization, waters were then added and further equilibrated for 5 ns using position restraints (10^3 kJ mol⁻¹ nm⁻²) on protein and phosphate beads of lipids. Because the relative orientation of the two helices was uncertain, two independent CG simulations were started by placing the TM regions of CD3 ϵ and CD3 δ in different relative orientations in each bilayer such that the charged residues Asp14 ϵ of the CD3 ϵ and Asp14 δ of the CD3 δ monomers lie either close or opposite to each other. Since neutralization of charges by substitution to polar residues (serine, asparagine) abrogates the assembly,^{6,8,9} both Asp14 ϵ and Asp14 δ were kept deprotonated, that is, each carries a total charge of -1 . For the self-association of TCR α –CD3 ϵ –CD3 δ trimer, the TCR α peptide was placed at about 50 Å away from the CD3 ϵ –CD3 δ dimer in a pre-equilibrated bilayer consisting of 275 POPC lipids, as in case of dimer. The trimer–micelle assembly simulation was carried out by combining the TCR α –CD3 ϵ –CD3 δ trimer with randomly positioned 100 dodecylphosphocholine (DPC) detergent molecules.

For comparison, a coarse-grained simulation of NKG2C–DAP12–DAP12 trimer (PDB entry 2L35.pdb) was also carried out in POPC bilayer. One of the 15 NMR models (model 13) was selected on the basis of ease of placing the protein in the membrane such that the termini did not bend back into the membrane. The trimer consisted of residues 1–32 of chains A and B and 38–61 of chain A from the 2L35.pdb entry. In the trimer, the DAP12 dimer is covalently linked via a disulfide bridge, whereas the NKG2C is included as an independent helix. This trimer was converted into a coarse-grained representation and then placed in a pre-equilibrated POPC bilayer or with randomly positioned 100 DPC molecules, as above. The size of the systems and time scale of the simulations are listed in Table 1.

Coarse-Grained Simulations. The MARTINI forcefield was used to carry out coarse-grained (CG) simulations.^{24,25} Initially the atomistic model of each peptide was converted to a CG representation based on four-to-one mapping, that is, on average four non-hydrogen atoms are represented by a single particle.^{24,25} The CG peptides were then inserted in a pre-equilibrated lipid bilayer. Counterions were added, where necessary, to preserve charge neutrality.

The simulations were carried out under periodic boundary conditions. The Berendsen's weak-coupling algorithm²⁶ was applied to set the pressure (1 atm) and the temperature using a coupling time of 1.0 ps. The temperature was maintained at 310 K for POPC and 325 K for DPPC simulations, well above their respective phase transition temperatures (278 and 315 K).^{27,28} For the protein–bilayer system a semi-isotropic pressure coupling scheme was employed. A

Table 1. Summary of Simulations

type	components	total particles or atoms	simulation time (ns) × replicas
CG ^a	CD3ε + CD3δ + 122 DPPC bilayer	9068	3000 × 2
CG	CD3ε + CD3δ + 128 POPC bilayer	8896	3000 × 2
CG	TCRα + CD3ε-CD3δ + 275 POPC bilayer	16394	3000 × 3 + 2000 × 2 ^b + 2000 × 12 ^c + 2000 × 12 ^d
AT ^e	TCRα-CD3ε-CD3δ + 184 POPC bilayer	42336	60 × 1 + 20 × 6 ^f
AT	TCRα-CD3ε-CD3δ + 275 POPC bilayer	65713	20 × 6
CG	TCRα-CD3ε-CD3δ + 100 DPCs	19297	2000 × 6
CG	NKG2C-DAP12-DAP12 + 174 POPC bilayer	9258	2000 × 1
CG	NKG2C-DAP12-DAP12 + 100 DPCs	19277	2000 × 1
AT	TCRα-CD3ε-CD3δ + 70 DPCs	58140	20 × 2
AT	NKG2C-DAP12-DAP12 + 65 DPCs	57786	20 × 2

^aCoarse-grained simulations. ^bTwo sets of simulations were run with different orientation of TCRα wrt CD3ε-CD3δ dimer. ^cCD3δ helix was rotated in 30° increments along the helix axis. ^dMutant dimers of CD3ε-CD3δ, viz., Asp14ε-Asn14δ, Asn14ε-Asp14δ, Asn14ε-Asn14δ, and Ala14ε-Ala14δ in triplicate. ^eAtomistic simulations. ^fAsn14ε-Asp14δ, Asn14ε-Asn14δ, and Ala14ε-Ala14δ mutant dimers of CD3ε-CD3δ, in duplicates.

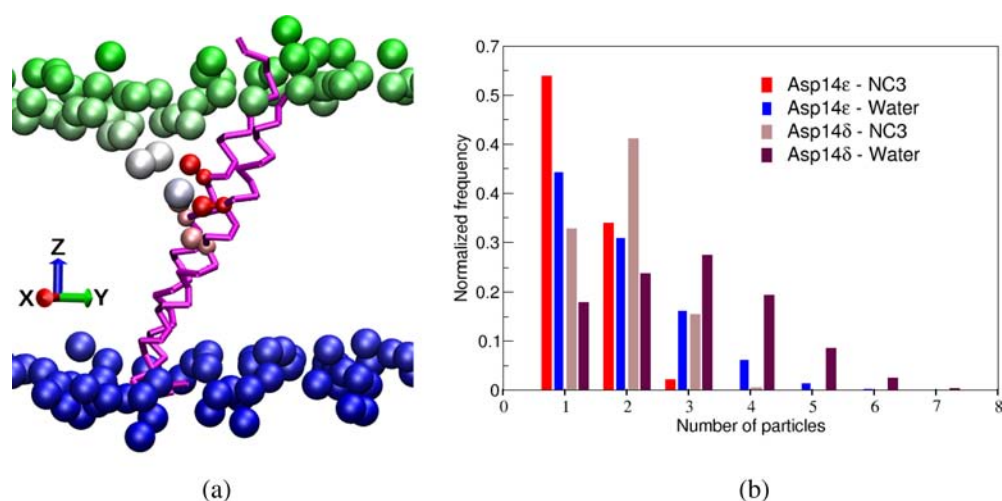


Figure 2. Structure and interactions of CD3ε-CD3δ dimer in a POPC bilayer. (a) Interaction of the choline headgroup with the Asp14ε-Asp14δ pair (red) of the dimer (purple). The choline moieties are colored according to their relative position along the bilayer normal (blue to green). (b) Normalized frequency of number of choline (red, tan) and water (blue, brown) particles within 6 Å of Asp14ε and Asp14δ from the two independent simulations.

temperature of 300 K and anisotropic pressure coupling was used for the protein-micelle system. Nonbonded interactions were cut off at 12 Å using a switching function distance at 9 Å for the LJ interactions and 0 Å for the Coulomb interactions. Pair lists were updated at least once every 10 steps. The waters were treated by a using polarizable CG water model²⁹ with a relative dielectric screening parameter set to 2.5. The equations of motion were integrated employing a time step of 20–30 fs. The coordinates and energies were saved every 200 ps. The size of the systems and time scale of the simulations are listed in Table 1.

Reconstruction of Atomistic Model from CG Representation. The reconstruction of CG model to atomistic (AT) model was done in two ways. In the first procedure, the peptides were converted to an atomistic model following a previously described methodology.^{30,31} Briefly, Pulchra software³² was used to build initial atomistic models of the assembled trimer using the CG protein backbone and side chain coordinates as the template. With this initial model as template, ten models were generated using Modeller. The model with lowest objective score was chosen for atomistic simulations. The TCRα-CD3ε-CD3δ trimer, after converting it to an atomistic model from a structure obtained from the CG simulations, was then inserted into a pre-equilibrated atomistic model of lipid bilayer using the InflateGRO method.³³ The atomistic simulations were carried out in POPC membrane only. Subsequently, the system was solvated with SPC waters. As in the CG simulations, the waters in the interior of bilayer were removed and counterions were added to preserve

neutrality. The system was subjected to 1000 steps of steepest descent energy minimization and 1 ns of molecular dynamics (MD) using a weak position restraint (10^3 kJ mol⁻¹ nm⁻²) on the non-hydrogen protein atoms. This was followed by a 60 ns unrestrained production run. In the second procedure, multiple CG representations were transformed into AT representations using a restrained simulated annealing procedure.³⁴ A CG structure was converted into two AT structures by using two different run times for decoupling CG restraints and equilibration. Three different CG simulation snapshots were converted, thus generating six starting AT structures in total. This was followed by a 20 ns unrestrained production run for each AT model.

To reconstruct the micellar system, a CG snapshot was converted to AT representation using the restrained simulated annealing procedure.³⁴ To reduce the system size, only the DPC and water residues whose atoms were within 17 Å were kept. The system was then placed in a cubic box with side length of 86 Å and solvated with water. After the minimization and equilibration, a 20 ns unrestrained production run was carried out for each AT model, as above.

Atomistic Simulation Procedure. Atomistic simulations were completed with the ffG53a6 force field³⁵ and Berger parameters³⁶ for lipid tails. A 2 fs time step was employed. The simulations were carried out under periodic boundary conditions. Bond lengths were constrained using the LINCS algorithm.³⁷ Water molecules were described using the SPC model.³⁸ The temperature was controlled by separately coupling the protein, lipids, and water to a heat bath at a

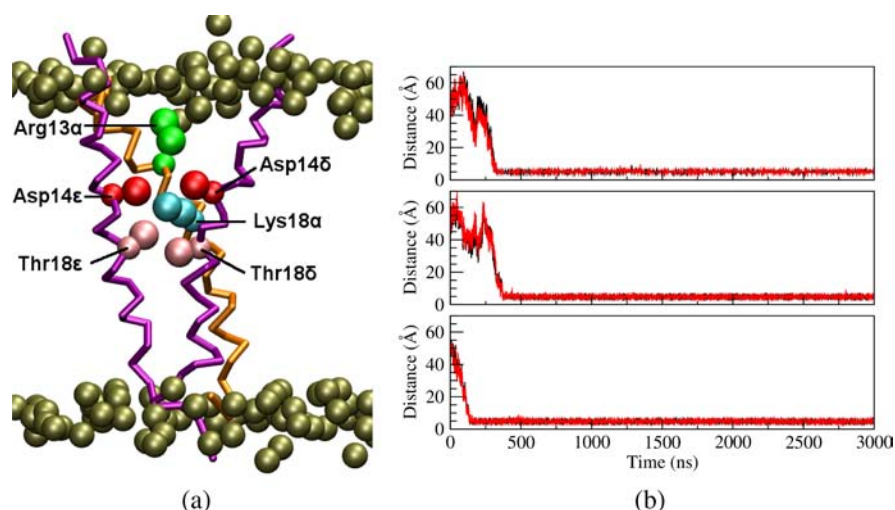


Figure 3. The self-assembly of the trimer in a POPC membrane. (a) A snapshot of the trimer showing close interaction between side chains of aspartic acid and threonine residues of CD3 ϵ –CD3 δ dimer (purple) and Lys18 α of the TCR α (orange). The membrane is represented as beads corresponding to the phosphate moiety of POPC. Also shown is the side chain of Arg13 α . (b) The evolution of distance between side chain beads of Lys18 α and Asp14 ϵ (black) and Lys18 α and Asp14 δ (red).

temperature of 310 K using the Nose–Hoover thermostat.^{39,40} The pressure was set at 1 atm using the Parrinello–Rahman barostat.⁴¹ A semi-isotropic coupling scheme was employed, wherein the lateral and perpendicular pressures are coupled independently at 1 bar. Lennard–Jones interactions were cutoff at 12 Å. Long-range electrostatics was handled by means of the particle-mesh Ewald method with cut off at 12 Å.

RESULTS

Structure of CD3 $\epsilon\delta$ Dimer in Model Membranes. The transmembrane domains of CD3 ϵ and CD3 δ were modeled as helices, converted to representative CG models, and then placed in a pre-equilibrated palmitoyl-oleoyl phosphatidylcholine (POPC) and dipalmitoyl phosphatidylcholine (DPPC) CG bilayers (see Computational Details). In the POPC membrane model, throughout the simulation length, the monomers remained close and parallel to each other. The dimer adopted a tilted orientation with respect to the bilayer normal with a mean tilt angle of about 26° and 22° for CD3 ϵ and CD3 δ , respectively. A snapshot of the last frame of the trajectory is shown in Figure 2a. The orientation of the dimer was similar in the DPPC bilayer, as judged by the mean tilt angle of 27° for CD3 ϵ and 24° for CD3 δ chains in the DPPC membrane (see Figure S1 in Supporting Information). The mean crossing angle of the helices was found to be ~11° in both bilayers. Thus, only the results from POPC membrane simulations are presented below.

Of primary interest was to understand how the TM acidic pair of the dimer is oriented and stabilized in the membrane environment. Visualization of the trajectories showed that the side chains of the Asp14 ϵ and Asp14 δ of the two helices tend to remain fairly close to each other, irrespective of their initial orientation and the repulsive Coulomb interaction between them. It is interesting to note that the lower leaflet of the bilayer is marginally disturbed (Figure 2a), while there is a considerable local deformation in the upper leaflet of the membrane with the lipid head groups penetrating the hydrophobic core of the bilayer. The aspartic acid pair is seen to be solvated by the penetrating lipid head groups and waters.

The interparticle contacts between side chains of acidic residues and the choline headgroups of lipids and waters were

analyzed employing a distance cutoff of 6 Å (see Figure 2b). The analysis was done on 5000 frames, taken at 200 ps intervals, from the last 1 μ s of each simulation trajectory. Figure 2b clearly shows that there is at least one choline group in contact with each acidic residue indicating that the lipids indeed penetrate the bilayer. The “pulled-in” lipid head groups appear to provide an important structural role in stabilizing the Asp14 ϵ –Asp14 δ pair of the dimer. To quantify a possible stabilizing effect of the penetrating lipid head groups, the average lifetime of the interaction between choline and the side chain of one of the two acidic residues was analyzed. This was computed by measuring how long a particular choline is within 6 Å of an aspartic acid side chain. Although the individual choline group involved in the choline–aspartic acid salt bridge changed during the simulation, the analysis did indicate that the mean lifetime of a particular choline–aspartic acid pair was about 23 ns. The longest lifetime found was 158 ns. The lifetime was also analyzed for the choline–aspartic acid interaction, such that a particular choline group is in contact with both Asp14 ϵ and Asp14 δ . It is interesting to note that during the aforementioned 158 ns, the Asp14 ϵ –choline–Asp14 δ existed for more than 86% of the time. Call and Wucherpfennig¹ previously proposed that the Asp14 ϵ and Asp14 δ jointly form a site for interaction with the TM lysine residue of TCR α .

Additionally, Figure 2 shows that there also is a significant number of contacts between the acidic residues and the waters throughout the simulation time. This further substantiates that indeed there is a local bilayer deformation for at least the entire length of the simulation used for the analysis.

Self-Assembly of Trimer. The TCR α helix and the CD3 ϵ –CD3 δ dimer were placed in a preformed POPC bilayer such that the centers of mass of the backbone beads of TCR α helix and the CD3 ϵ –CD3 δ dimer were about 50 Å apart. Three independent simulations, each starting with a different set of velocities, were carried out for 3 μ s. These simulations allowed the helices to diffuse through the membrane and self-assemble. It was observed that the trimer was formed spontaneously, within a few hundreds of nanoseconds and lasted throughout the remainder of the simulation.

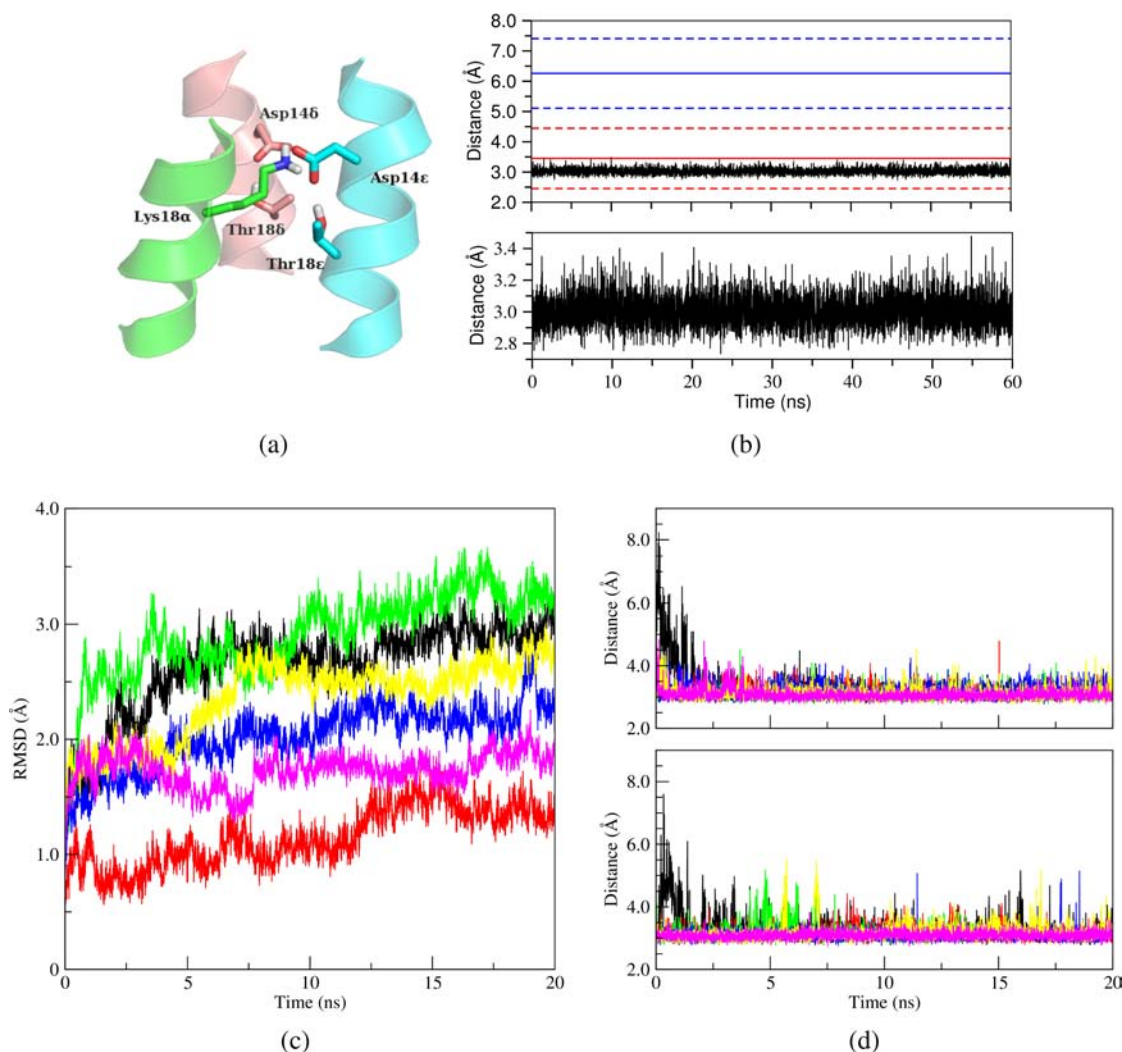


Figure 4. AT simulation of TCR α -CD3 ϵ -CD3 δ trimer. (a) A snapshot showing the interactions among the TM charged residues. (b) Minimum distance between N ζ atom of Lys18 α and O δ atoms of Asp14 ϵ (black, upper panel) and Asp14 δ (lower panel). Also shown is the mean (solid) and standard deviation (dashed) of the distance between N ζ atom of Lys18 α of NKG2C and the closest O δ atom of the two aspartic acids of DAP12 dimer (red, blue) from the NMR ensemble of structures (PDB 2L35). (c, d) The simulations based on restrained simulated annealing transformation of CG structure. (c) The rmsds of the C α atoms of TM helices of the trimer. (d) The minimum distance between Lys18 α , atom N ζ , and Asp14 ϵ , O δ atoms (upper panel), and Asp14 δ , O δ atoms (lower panel).

A snapshot of the assembled TCR α -CD3 ϵ -CD3 δ trimer is shown in Figure 3a. In contrast to the dimer simulations (Figure 2), there is no penetration of lipid head groups into the interior of the bilayer. The CD3 ϵ and CD3 δ peptides lie at an angle to each other with a modal crossing angle of about 40°, with the Asp/Glu-XX-Thr motif acting as a pivot. The aspartic acid and threonine side chains of the motif lie on the same face of the CD3 ϵ -CD3 δ dimer. Interestingly, the Lys18 α of TCR α occupies a very similar position as the choline group observed in the simulation of CD3 ϵ -CD3 δ dimers (Figure 2a). The lysine residue interacts with the negatively charged acidic pair. A visualization of the trajectory shows that these interactions are persistent in the trimer throughout the simulations. The trajectories were then analyzed for the evolution of minimum distance between side chains of lysine and aspartic acids of the dimer, Figure 3b. Also, the spatial distribution and the crossing angles of the CD3 ϵ and CD3 δ helices, with respect to TCR α were used as a measure for the convergence of simulations. The analysis indicated that the structure of the trimer converged within 1 μ s of simulation (also see Figures S2–S4, Supporting

Information). It is worth mentioning that, although during the initial stages of self-assembly, the Arg13 α side chain occasionally interacted with one of the TM aspartic acid residues of the dimer, it is primarily involved in an interaction with the phosphate group of the upper leaflet of the lipid bilayer. This finding confirms the previous mutational studies on the importance of Lys18 α in the assembly of TCR α -CD3 ϵ -CD3 δ trimers.^{6,42}

To evaluate the key interactions involved in the trimer assembly, the interhelical contacts were analyzed. Residue-residue contact maps were calculated based on the minimum distance between interhelix residues and averaged over the last 1 μ s of the simulations (see Figure S5, Supporting Information). The analysis revealed that, besides the strong electrostatic interactions between the Lys18 α and Asp/Glu-XX-Thr motif, the association is also driven by prominent interactions at the C-terminus. Of these, the most notable are Phe22 α -Leu22 ϵ , Met26 α -Ile25 ϵ , Arg29 α -Tyr26 ϵ , Leu25 α -Leu19 δ , and Arg29 α -Tyr26 δ . These findings provide substantial support to a recent study that demonstrated that the

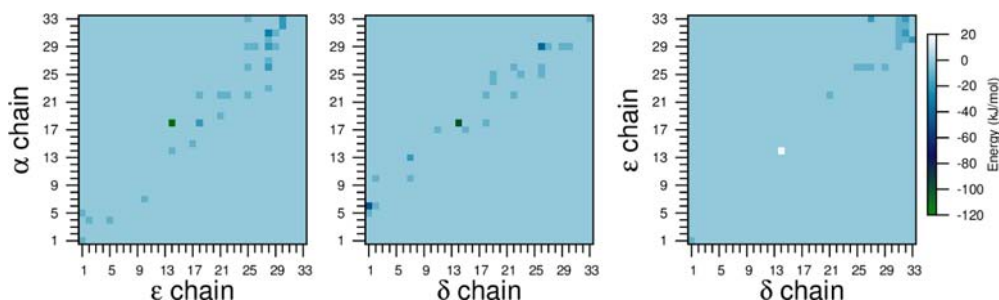


Figure 5. A crude estimate of residue-based interaction energies between TCR and CD3. The time-averaged interaction energy between TCR α and CD3 ϵ (left panel), TCR α and CD3 δ (middle panel), and CD3 ϵ and CD3 δ residues (right panel) are shown.

truncation of the C-terminal end of the TM region of TCR α abrogates the assembly of the TCR–CD3 complex.⁴³ Additionally, Leu22 ϵ –Ala22 δ , Met23 ϵ –Val25 δ , and Tyr26 ϵ –Tyr26 δ are the close interactions between CD3 heterodimer units.

To obviate the possibility of an effect of initial positioning of helices on assembly, two additional sets of simulations were carried out. In the first set, two independent simulations were started wherein the orientation of TCR α was flipped. The results of these simulations were very similar. In the other set, the TCR α and CD3 ϵ were kept at the same initial position, while the CD3 δ helix was rotated in 30° increments in 12 independent simulations. The analysis of the spatial distribution of the helices, carried out as above, showed a similar probability density of the helices (Figure S6, Supporting Information). Further, the distances between Lys18 α and aspartic acid side chains were also analyzed (see Figure S7, Supporting Information). In all of the simulations, except for the one with CD3 δ at 300°, these distances were identical to the above simulations. In the simulation with CD3 δ at 300°, lysine was interacting with the phosphate groups of the bilayer (Figure S8, Supporting Information). The aspartic acids of the CD3 dimer were seen to be interacting with the choline head groups of the bilayer, just as in the case of CD3 dimer alone (Figure 2a). As expected from the spatial distribution, the orientation of CD3 helices with respect to the TCR α chain appear to be similar.

In order to gain detailed insights and, more importantly, to evaluate the interactions among the TM charged residues, the CG representation of the protein was converted to an atomistic representation. To eliminate any bias, the AT model of trimer was inserted into a pre-equilibrated POPC bilayer and simulated for a sufficiently long time (60 ns) to ensure stability and good sampling. The atomistic simulations showed that each of the TM region chains was stable in the bilayer and adopted predominantly an α -helical structure (data not shown). The polar interaction site of AT structure of TCR α –CD3 ϵ –CD3 δ trimer in bilayer was then compared with the micellar NMR structure of NKG2C–DAP12–DAP12 trimer (2L35 pdb). This comparison clearly shows that both the acidic residues of TCR α –CD3 ϵ –CD3 δ are much closer to the lysine residue (Figure 4a,b). The AT simulation further confirmed the interactions identified by the CG simulations. Importantly, both acidic residues were hydrogen bonded to intrachain threonine residues and formed a stable salt bridge with the Lys18 α .

In addition, the CG particles were transformed to an atomistic representation using a restrained simulated annealing procedure. Because of the large size of the system, six independent, short (20 ns) simulations were carried out from different starting structures. Figure 4c shows that C α root mean

squared deviations (rmsd) stabilized rapidly to a small rmsd, indicating a stable membrane protein model. Interestingly, all AT simulations highlight a similar behavior of the acidic and basic residues in a bilayer (Figure 4d).

From all AT simulations, the last 10 ns trajectories were gathered and merged, and the short-range nonbonded potential interaction energy between the interchain residues was calculated, as described elsewhere.⁴⁴ These energies are a crude estimate and incomplete because the long-range electrostatics and reaction field effects are not taken into account. These energies are not related to any experimental observables. The plots (Figure 5) show that Lys18 α strongly interacts with both the acidic residues, Asp14 ϵ (–114 kJ/mol) and Asp14 δ (–105 kJ/mol). The standard deviations were 48.2, 17.1, and 44.3 kJ/mol for total interaction energy and van der Waals and electrostatic terms, respectively.

Effect of Asp14 Mutations on Trimer Assembly. As mentioned before, experimental studies have shown that the deletion of negative charge upon mutations to asparagine or alanine lead to significant reduction in assembly of the trimers of various activating immunoreceptors.^{1,6,8,9} To explore the effect of mutants on the assembly of the trimers, self-assembly of Asp14 ϵ –Asn14 δ , Asn14 ϵ –Asp14 δ , Asn14 ϵ –Asn14 δ , and Ala14 ϵ –Ala14 δ mutants were also carried out. The spatial distribution analysis for each mutant trimer indicates that the mutants fail to assemble in a mode as observed for the wild-type system studied above (Figure S9, Supporting Information).

Further, to assess the effect of these mutations at an atomistic level, a snapshot (at 40 ns, Figure 4b) from the wild-type AT simulation was taken and converted into Asn14 ϵ –Asp14 δ , Asn14 ϵ –Asn14 δ , and Ala14 ϵ –Ala14 δ mutant trimers. Two independent AT simulations were done for each mutant. The RMSD analysis of the trimer (Figure S10, Supporting Information) clearly shows that these mutations destabilize the trimer assembly, as seen in the corresponding CG simulations.

Protonation State of Lys18 and Asp14 Residues. The biochemical⁶ and structural studies⁸ have suggested that the lysine and aspartic acid residues are charged in the assembled trimer. One could argue that initially the lysine enters the membrane as a neutral species along with neutral acidic residues, and during the assembly of the trimer, one of the aspartic acids donates its proton to the lysine resulting in an ion pair and a neutral acidic residue. Further simulations, in addition to those listed in Table 1, were carried out to investigate the protonation state of the key residues involved in the trimer assembly. Initially, self-assembly coarse-grained simulations were carried out with both the aspartic acids and

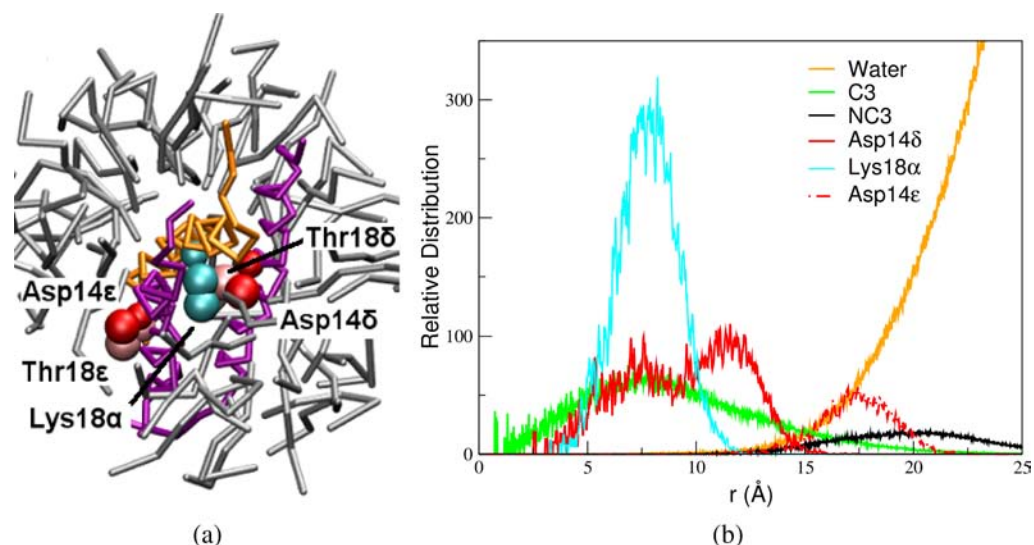


Figure 6. Analysis of TCR α -CD3 ϵ -CD3 δ structure in a micelle. (a) Snapshot of trimer in DPC micelle. DPCs are shown in gray. Coloring scheme for protein is same as in Figure 2. (b) Distribution of water, choline (NC3), tail atoms of DPCs (C3), Lys18 α , and Asp14 of ϵ and δ chains with respect to micelle core (about 40 DPCs).

the lysine in neutral states (Lys18 α^0 -Asp14 ϵ^0 -Asp14 δ^0). The spatial distribution of the helices, obtained from three independent self-assembly simulations (Figure S11A, Supporting Information), appear very similar to those seen for the Asn14 ϵ -Asn14 δ mutant (Figure S9, Supporting Information). Also, the evolution of minimum distance between Lys18 α^0 and Asp14 side chains showed that the Lys18 α^0 does not stably interact with either of the neutral acidic residues (Figure S11B, Supporting Information) when compared with the residues in charged state (see Figure 3b).

Simultaneously, two sets of 500 ns long coarse-grained simulations were carried out with Lys18 α^+ -Asp14 ϵ^- -Asp14 δ^0 and Lys18 α^+ -Asp14 ϵ^0 -Asp14 δ^- charge states, starting with a snapshot from the aforementioned coarse-grained self-assembly simulation. The distance analysis strongly suggests that neutralizing the charge on the acidic residues destabilizes its interaction with Lys18 α^+ side chain (see Figure S12A, Supporting Information). The figure also shows that the atomistic simulations, initiated from the coarse-grained simulations, similarly indicate a destabilized interaction. The analysis of hydrogen bond existence on the atomistic simulations show that the neutral Asp14 rather forms a strong hydrogen bond with the negatively charged Asp14 and not with the intrachain threonine residue (Figure S12B, Supporting Information).

Micelle versus Membrane Environment. Previous studies have shown that there are more dynamic fluctuations in a micelle compared with a bilayer environment.^{45,46} It is quite likely that the observation of the relative position of the acidic residues of the DAP dimer, with only one of them in direct contact with the basic residue, is essentially because the structure was solved in a micelle environment. Thus it was imperative to compare and contrast the structure of the assembled TCR α -CD3 ϵ -CD3 δ trimer in POPC bilayer to that of in a micelle environment. Six simulations were initiated from three different trimer structures obtained from self-assembly simulations in POPC bilayer. These trimers were placed in a box with 100 randomly placed dodecylphosphocholine (DPC) molecules. Each simulation of micelle formation around the trimer was carried out for 2 μ s.

It was observed that about 50 DPC molecules associated with the trimer within 50 ns of simulation. The visual inspection of the trimer-micelle complex indicated that trimer remains partially buried for the entire length of the simulation (Figure 6a). The relative position of various atoms with respect to the center of the micelle core can be seen quantitatively in the radial distribution plot (Figure 6b). The results from all the micelle simulations were identical (also see Figure S13, Supporting Information). From these distribution plots, it can be seen that the side chain of Lys18 α lies near the core of the micelle, occupying a similar position as of C3 atoms of DPCs forming the inner core of the micelle. However, only Asp14 δ appears to lie close to the Lys18 α , while the Asp14 ϵ “snorkels-out” to interact with the choline headgroup of DPCs and the bulk solvent.

Simultaneously, the CG simulations of the NMR structure of NKG2C-DAP12-DAP12 trimer were also carried out in a POPC bilayer and micelle environments. Interestingly, the resulting structure from the simulations of NKG2C-DAP12-DAP12 trimer in a POPC bilayer (Figure 7b) showed that the arrangement of the acidic and threonine residues of DAP12 homodimer with respect to lysine of NKG2C is very similar to the TCR α -CD3 ϵ -CD3 δ trimer in the bilayer (Figures 3 and 4). Further, the simulations of NKG2C-DAP12-DAP12 trimer in a micelle clearly indicated that the interaction of both acidic residues and lysine is markedly stable only in a membrane (see Figure 8). Only one of the acidic residues of DAP12 dimer strongly interacts with the lysine of NKG2C, while the other acidic residue predominantly interacts with the choline headgroup of DPCs and the waters. Starting from a CG structure extracted from the coarse-grained micelle simulations of both the trimers, AT models were generated using the restrained simulated annealing procedure.³⁴ The interactions of the acidic residue with the detergent head groups and bulk water were found to be stable in multiple atomistic simulations (see Figure S14, Supporting Information).

Overall, the results convincingly demonstrate that in a bilayer environment, the two helices are oriented such that the Asp14 ϵ -Asp14 δ pair lie at the same face of the dimer and are in close interaction with the Lys18 α of the third helix of the

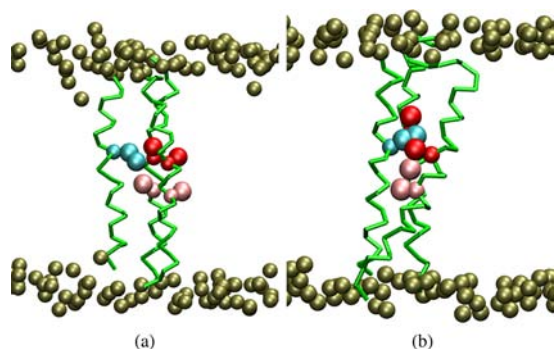


Figure 7. NKG2C–DAP12–DAP12 trimer in a POPC bilayer. (a) NMR model of the trimer (PDB 2L35; model 13), converted to a CG model and placed in a bilayer at the start of simulation. (b) A snapshot of the configuration at approximately 2.5 μ s. The side chains of aspartic acids (red), threonine (pink), and lysine (cyan) residues are shown as spheres. The phosphate groups (tan) of the POPC membrane are also shown as spheres.

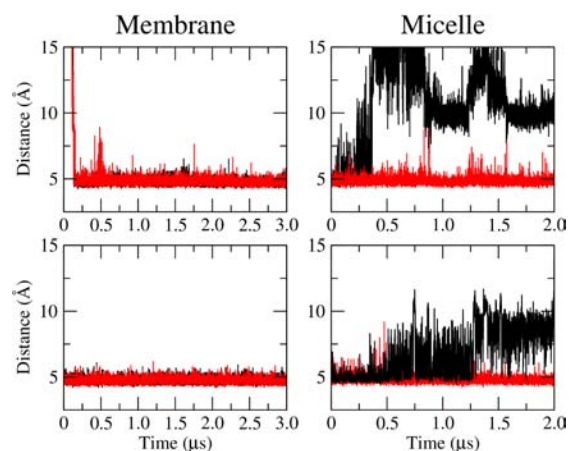


Figure 8. Interaction among the charged residues in membrane and micelle environments. The minimum distance between lysine and Asp14 ϵ (red) and Asp14 δ (black) based on TCR α –CD3 ϵ –CD3 δ simulations in POPC membrane (top left) and in DPC micelles (top right). The distance between lysine and two acidic residues from the simulations of NKG2C–DAP12–DAP12 trimer in POPC membrane (lower left) and in DPC micelles (lower right).

trimer (Figure 8). In contrast, the micelle simulations show that only Asp14 δ is involved in contact with the Lys18 α , while the Asp14 ϵ interacts primarily with choline group of DPCs of the micelle.

DISCUSSION

To gain insight into T cell receptor mediated signaling, the first and foremost question to ask is how the trimers are assembled and stabilized in a membrane environment. The simulation studies in the present work have shown that in a membrane the TM helices of CD3 ϵ and CD3 δ adopt a tilted orientation. It is remarkable to note that the two transmembrane acidic residues are predominantly positioned at the same face of the dimer. Further, the electrostatic repulsion between these closely placed acidic residues in a low dielectric environment is neutralized by the formation of salt bridges with a choline headgroup of the penetrating lipids, as judged by the bilayer deformation and the persistence of the interactions during the simulations of the dimer in a POPC membrane.

In the modeled TCR α –CD3 ϵ –CD3 δ trimeric structure, the TCR α helix is positioned such that, of the two positively charged residues, only Lys18 α was found to lie in the interior of the membrane whereas the side chain of Arg13 α appears to snorkel out of the membrane interior and interact with the phosphate groups of the lipids lying at the membrane–water interface. On the basis of this, it can be speculated that residue Lys18 α , which lies in the membrane interior, and not Arg13 α would prevent the homo-oligomerization of TCR α . Upon mutation of the charge of Lys18 α , TCR α homo-oligomers would be able to form and consequently escape degradation. Thus, these results appear to be in agreement with the experimental finding on the dispensability of Arg13 α for degradation of TCR α .⁴⁷

Comparing the modeled membrane structure of TCR α –CD3 ϵ –CD3 δ with a recently solved NMR structure highlights significant similarities and differences. The NMR structure of NKG2C–DAP12–DAP12 trimer shows that of the two aspartic acids in the Asp-XX-Thr motifs only one is in direct interaction with the lysine, while both acidic residues are hydrogen bonded to the intrachain threonine of the Asp-XX-Thr motif. Experimental evidence demonstrates that mutations of the threonine residues abrogate the trimerization but have no effect on the formation of dimers.⁸ The membrane structure of TCR α –CD3 ϵ –CD3 δ trimer shows that the amine group of Lys18 α occupies a very similar position to the choline in the CD3 ϵ –CD3 δ dimer. The Lys18 α side chain simultaneously interacts with Asp14 ϵ and Asp14 δ , in contrast to the NMR structure. The acidic residues form strong intramolecular hydrogen bonds with Thr18 ϵ and Thr18 δ , similar to the NMR structure, and thus assign a direct role to the threonines in trimer association. As noted previously,⁸ the establishment of such an electrostatic network is important for the assembly of the trimer. Further, the simulations suggest that the neutralization of negative charge, either by protonation or by mutation to an uncharged residue, has a detrimental effect on the trimer assembly by destabilizing its interaction with the positively charged lysine or a reduced persistence of the Asp14–Thr18 hydrogen bond.

In contrast to a membrane environment, contacts with water are more prominent in a micelle. The modeled structure of TCR α –CD3 ϵ –CD3 δ trimer when placed in micelle environment shows that at least one of the aspartic acid residues is in contact with bulk solvent because the polar solvent tends to screen electrostatic interactions. Consequently, the formation of an Asp–Lys–Asp triplet is less likely to occur because the stabilizing lysine residue is less strongly interacting with the aspartic acid residues. Thus, the two aspartic acid residues are more likely to move away from each other, even though the electrostatic repulsive interaction between them is diminished by the presence of a positively charged lysine residue. Consequently, only one of the acidic residues of the dimeric Asp-XX-Thr motif is in contact with the lysine, while the other acidic residue appears to be highly solvated by the bulk solvent. A vice versa scenario, where the micellar structure of the NKG2C–DAP12–DAP12 trimer was placed in a model bilayer, confirms the model of TCR α –CD3 ϵ –CD3 δ trimer. Here again, the lysine of NKG2C interacts with Asp-XX-Thr motifs on both the side chains of DAP12 homodimer.

Previous computational studies on TM dimers, such as glycoporphin⁴⁸ and integrins,¹⁴ have shown that there are significant difference between the structures modeled in membrane compared with experimental NMR structures.

These proteins are largely hydrophobic. The current study on charged TM segments highlights that the differences in membrane and NMR structures could be more pronounced when charged residues are present in the TM regions. Whether it is true for other proteins requires further studies.

Specific helical interactions in transmembrane domains are the key to a proper assembly of many immune receptors.^{9,10} The previous model by Call et al.⁸ of trimer association, based on the NKG2C–DAP12–DAP12 micellar NMR structure, assumes a certain degeneracy, as noted in the Introduction. According to that model, a positively charged side chain can approach the oppositely facing negatively charged residues of the dimer from either side. This would result in the formation of an equal number of nonproductive and productive arrangements of the extracellular domains of the trimer. On the basis of the results from this work, we propose a revised model for trimerization (Figure 9). According to our model, the

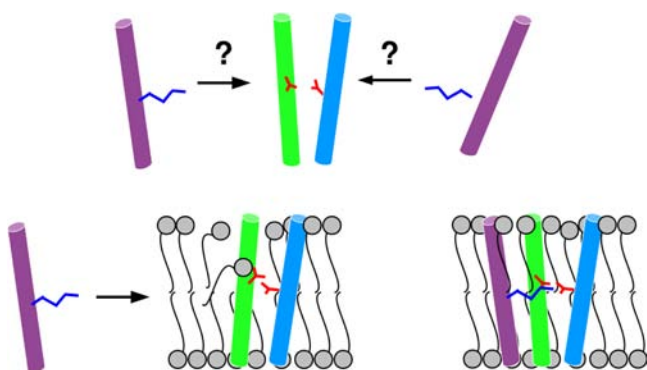


Figure 9. Model for the assembly of TM domains of immune receptors. The question marks highlight the degeneracy in the currently accepted model based on NMR structure of NKG2C–DAP12–DAP12 trimer (upper panel). The revised model based on this study (lower panel).

two aspartic acid residues are positioned on the same side of the dimer and are anchored by the threonine side chain via intrahelical hydrogen bonds. This orientation is further stabilized by the choline head groups of the membrane lipids penetrating the interior of the bilayer. During the trimer assembly, the monomer bearing a positively charged residue (a lysine, in case of TCR α) replaces this choline group, Figure 9. Thus, this new model eliminates the degeneracy and provides an explanation of the link between specific transmembrane interactions and the observed sidedness in the assembly of receptor complex.⁴⁹

■ ASSOCIATED CONTENT

● Supporting Information

Complete refs 21 and 49 and detailed analysis of MD simulations. This material is available free of charge via the Internet at <http://pubs.acs.org>.

■ AUTHOR INFORMATION

Corresponding Author

andre.juffer@oulu.fi

Notes

The authors declare no competing financial interest.

■ ACKNOWLEDGMENTS

We thank the Center for Scientific Computing-IT Center for Science Ltd., Espoo-FI, for providing computational resources. We acknowledge the Biocenter Oulu Biocomputing Core facility for financial support.

■ REFERENCES

- (1) Call, M. E.; Wucherpfennig, K. W. *Nat. Rev. Immunol.* **2007**, *7*, 841–850.
- (2) Weiss, A.; Littman, D. R. *Cell* **1994**, *76*, 263–274.
- (3) Rudolph, M. G.; Stanfield, R. L.; Wilson, I. A. *Annu. Rev. Immunol.* **2006**, *24*, 419–466.
- (4) Smith-Garvin, J. E.; Koretzky, G. A.; Jordan, M. S. *Annu. Rev. Immunol.* **2009**, *27*, 591–619.
- (5) Kuhns, M. S.; Davis, M. M.; Garcia, K. C. *Immunity* **2006**, *24*, 133–139.
- (6) Call, M. E.; Pyrdol, J.; Wiedmann, M.; Wucherpfennig, K. W. *Cell* **2002**, *111*, 967–979.
- (7) Call, M. E.; Wucherpfennig, K. W. *Annu. Rev. Immunol.* **2005**, *23*, 101–125.
- (8) Call, M. E.; Wucherpfennig, K. W.; Chou, J. J. *Nat. Immunol.* **2010**, *11*, 1023–1029.
- (9) Feng, J.; Garrity, D.; Call, M. E.; Moffett, H.; Wucherpfennig, K. W. *Immunity* **2005**, *22*, 427–438.
- (10) Manolios, N.; Bonifacio, J. S.; Klausner, R. D. *Science* **1990**, *249*, 274–277.
- (11) Fink, A.; Sal-Man, N.; Gerber, D.; Shai, Y. *Biochim. Biophys. Acta* **2012**, *1818*, 974–983.
- (12) Treptow, W. W.; Marrink, S. J.; Tarek, M. J. *Phys. Chem. B* **2008**, *112*, 3277–3282.
- (13) Periolo, X.; Huber, T.; Marrink, S. J.; Sakmar, T. P. *J. Am. Chem. Soc.* **2007**, *129*, 10126–10132.
- (14) Kalli, A. C.; Hall, B. A.; Campbell, I. D.; Sansom, M. S. *Structure* **2011**, *19*, 1477–1484.
- (15) Krogh, A.; Larsson, B.; von Heijne, G.; Sonnhammer, E. L. *J. Mol. Biol.* **2001**, *305*, 567–580.
- (16) Juretić, D.; Zoranić, L.; Zucić, D. *J. Chem. Inf. Comput. Sci.* **2002**, *42*, 620–632.
- (17) Cao, B.; Porollo, A.; Adamczak, R.; Jarrell, M.; Meller, J. *Bioinformatics* **2006**, *22*, 303–309.
- (18) Bonifacio, J. S.; Cosson, P.; Shah, N.; Klausner, R. D. *EMBO J.* **1991**, *10*, 2783–2793.
- (19) Xu, C.; Call, M. E.; Wucherpfennig, K. W. *J. Biol. Chem.* **2006**, *281*, 36977–36984.
- (20) Sali, A.; Blundell, T. L. *J. Mol. Biol.* **1993**, *234*, 779–815.
- (21) Berman, H. M.; et al. *Nucleic Acids Res.* **2000**, *28*, 235–242.
- (22) Hess, B.; Kutzner, C.; van der Spoel, D.; Lindahl, E. *J. Chem. Theory Comput.* **2008**, *4*, 435–447.
- (23) Humphrey, W.; Dalke, A.; Schulten, K. *J. Mol. Graphics* **1996**, *14*, 33–38.
- (24) Marrink, S. J.; Risselada, H. J.; Yefimov, S.; Tieleman, D. P.; De Vries, A. H. *J. Phys. Chem. B* **2007**, *111*, 7812–7824.
- (25) Monticelli, L.; Kandasamy, S. K.; Periolo, X.; Larson, R. G.; Tieleman, D. P.; Marrink, S. J. *J. Chem. Theory Comput.* **2008**, *4*, 819–834.
- (26) Berendsen, H. J. C.; Postma, J. P. M.; van Gunsteren, W. F.; Dinola, A.; Haak, J. R. *J. Chem. Phys.* **1984**, *81*, 3684–3690.
- (27) Litman, B. J.; Lewis, E. N.; Levin, I. W. *Biochemistry* **1991**, *30*, 313–319.
- (28) Nagle, J. F.; Tristram-Nagle, S. *Biochim. Biophys. Acta* **2000**, *1469*, 159–195.
- (29) Yesylevskyy, S. O.; Schäfer, L. V.; Sengupta, D.; Marrink, S. J. *PLoS Comput. Biol.* **2010**, *6*, No. e1000810.
- (30) Wee, C. L.; Gavaghan, D.; Sansom, M. S. *Biophys. J.* **2010**, *98*, 1558–1565.
- (31) Stansfeld, P. J.; Hopkinson, R.; Ashcroft, F. M.; Sansom, M. S. *Biochemistry* **2009**, *48*, 10926–10933.

- (32) Rotkiewicz, P.; Skolnick, J. *J. Comput. Chem.* **2008**, *29*, 1460–1465.
- (33) Kandt, C.; Ash, W. L.; Tieleman, D. P. *Methods* **2007**, *41*, 475–488.
- (34) Rzepiela, A. J.; Schä, L. V.; Goga, N.; Risselada, H. J.; De Vries, A. H.; Marrink, S. J. *J. Comput. Chem.* **2010**, *31*, 1333–1343.
- (35) Oostenbrink, C.; Villa, A.; Mark, A. E.; van Gunsteren, W. F. *J. Comput. Chem.* **2004**, *25*, 1656–1676.
- (36) Berger, O.; Edholm, O.; Jähnig, F. *Biophys. J.* **1997**, *72*, 2002–2013.
- (37) Hess, B.; Bekker, H.; Berendsen, H. J. C.; Fraaije, J. G. E. M. *J. Comput. Chem.* **1997**, *18*, 1463–1472.
- (38) Berendsen, H. J. C.; Postma, J. P. M.; Van Gunsteren, W. F.; Hermans, J. In *Intermolecular Forces*; Pullman, B., Ed.; Reidel: Dordrecht, The Netherlands, 1981; pp 331–342.
- (39) Nosé, S. *J. Chem. Phys.* **1984**, *81*, 511–519.
- (40) Hoover, W. G. *Phys. Rev. A* **1985**, *31*, 1695–1697.
- (41) Parrinello, M.; Rahman, A. *J. Appl. Phys.* **1981**, *52*, 7182–7190.
- (42) Blumberg, R. S.; Alarcon, B.; Sancho, J.; McDermott, F. V.; Lopez, P.; Breitmeyer, J.; Terhorst, C. *J. Biol. Chem.* **1990**, *265*, 14036–14043.
- (43) Shelton, G. J.; Gülland, S.; Nicolson, K.; Kearse, K. P.; Bäckström, B. T. *Mol. Immunol.* **2001**, *38*, 259–265.
- (44) Aponte-Santamaría, C.; Briones, R.; Schenk, A. D.; Walz, T.; de Groot, B. L. *Proc. Natl. Acad. Sci. U.S.A.* **2012**, *109*, 9887–9892.
- (45) Bond, P. J.; Sansom, M. S. *J. Mol. Biol.* **2003**, *329*, 1035–1053.
- (46) Johnston, J. M.; Cook, G. A.; Tomich, J. M.; Sansom, M. S. *Biophys. J.* **2006**, *90*, 1855–1864.
- (47) Soetandyo, N.; Wang, Q.; Ye, Y.; Li, L. *J. Cell Sci.* **2010**, *123*, 1031–1038.
- (48) Psachoulia, E.; Fowler, P. W.; Bond, P. J.; Sansom, M. S. *Biochemistry* **2008**, *47*, 10503–10512.
- (49) Kuhns, M. S.; et al. *Proc. Natl. Acad. Sci. U.S.A.* **2010**, *107*, 5094–5099.